Three-body systems with attractive $1/r$ potentials

J. P. D'Incao, S. C. Cheng, H. Suno, and B. D. Esry
Department of Physics, Kansas State University, Manhattan, Kansas 66506, USA
(Received 21 December 2005; revised manuscript received 26 January 2007; published 12 March 2007)

We have used the hyperspherical adiabatic representation to describe the system of three identical bosons in a spin stretched state interacting through an attractive $1/r$ potential. A proposal has been forwarded to enable the experimental realization of such a system in cold trapped atoms using extremely off-resonant laser fields [Phys. Rev. Lett., **84**, 5687 (2000)]. We have obtained the effective potentials, channel functions, and nonadiabatic couplings for this gravitylike interaction, allowing us to calculate the ground-state energy with accuracy that substantially improves upon previous results. We have similarly calculated the energies for the first four 0^+ excited states. These results show that the simple adiabatic hyperspherical approximation offers an accurate description for such a system. Further, since the effective potentials have a long-range $1/R$ attraction, the properties of the excited states follow from the well-known results for Rydberg states. We have also analyzed the possible geometries and vibrational modes for this system.

DOI: 10.1103/PhysRevA.75.032503 PACS number(s): 31.15.Ja, 32.10.−f, 34.20.Cf

I. INTRODUCTION

Recently, a scheme for inducing gravitationlike interatomic potentials has been proposed [1], opening up the possibility to create self-bound Bose-Einstein condensates (BECs) [2–6]. In such a scheme, the gravitationlike interatomic potential can be achieved by irradiating the atoms with intense, extremely off-resonant electromagnetic fields. The usual strong anisotropy due to dipole-dipole interactions can, in fact, be averaged out [7] by the proper combination of laser beams, leaving a $-u/r$ potential, where u is the strength of the potential (the analog of GMm, where G is the Newton's constant and M and m are the masses) and r is the interparticle distance. The strength u of the potential can be adjusted by changing the laser intensity [1].

In ultracold atomic gases, two interesting regimes for self-bound BECs have been predicted, assuming that the short-range interatomic interactions can be independently tuned by, say, applying a magnetic field near a Feshbach resonance [8]. In one regime, the attractive $1/r$ interactions are balanced by the repulsive mean-field interaction assuming a positive two-body scattering length and negligible kinetic energy. In the other regime, the balancing factor is kinetic energy, assuming negligible mean-field interactions. In both regimes, the resulting BEC is self-bound. From a broader point of view, the induced gravitationlike interaction might make possible experimental emulation of boson stars (a system of self-gravitating bosons) in the regime where the kinetic energy balances the $-u/r$ potential [9,10]. Moreover, purely attractive $1/r$ potentials constitute an interesting contrast to the attractive and repulsive Coulomb potentials atomic physicists are used to.

The existence of a lower bound for the ground-state energy in many-body systems interacting through attractive $1/r$ potentials is of fundamental importance in order to prove the existence of the thermodynamical limit and the stability of normal matter [11]. It was shown in Ref. [12] that for a system of N identical, spinless (or spin stretched) bosons of mass m interacting gravitationally, the lower and upper bounds for the ground-state energy are, respectively, $-\frac{1}{16}N^2(N-1)G^2m^5/\hbar^2$ and $-0.0542N(N-1)^2G^2m^5/\hbar^2$, where the upper bound was obtained variationally. For small N, however, the discrepancy between the lower and upper bounds becomes large. For $N=3$, using a more refined trial function, they obtained $-0.954\,92G^2m^5/\hbar^2$ for the upper bound, representing a difference of about 15% between the upper and lower, $(-\frac{9}{8}G^2m^5/\hbar^2)$, bounds and a ground-state energy equal to $E_0 \cong -1.067G^2m^5/\hbar^2$.

In this paper, we have used the adiabatic hyperspherical representation for this system to obtain effective three-body potentials, the corresponding channel functions, and the nonadiabatic couplings. Using these, we calculate the ground state and low-lying 0^+ excited state energies converged to seven digits. We have also used the adiabatic hyperspherical representation to obtain lower and upper bounds that differ by about 0.1%, indicating that a simple single-channel description offers a quite accurate description of such systems. Additionally, we have determined from the asymptotic behavior of the effective three-body potentials that the 0^+ bound states for three-body systems with attractive $1/r$ interactions are Rydberg states. All of the knowledge we have gained for Rydberg states in atomic systems can thus be directly transferred to this three-body system. We have also used the channel functions to analyze the geometry and vibrational modes for both bound and resonant states. We have found that all 0^+ bound states are breathing modes, while the 0^+ resonant states have contributions from both bending and breathing modes. The breathing-mode component dominates, however, for the low-lying resonances we examined.

II. THE ADIABATIC HYPERSPHERICAL REPRESENTATION

We have solved the Schrödinger equation in hyperspherical coordinates. After separation of the center-of-mass motion, the system is described by the hyperradius R which gives the overall size; three Euler angles α, β, and γ, specifying the orientation of the plane containing the three particles relative to the space-fixed frame; and two other hyperangles φ and θ, describing the internal relative motion

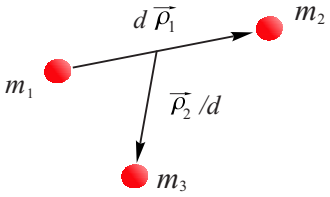

FIG. 1. (Color online) The mass-scaled Jacobi coordinates for systems with three particles.

between the particles. The angles φ and θ are modified Smith-Whitten coordinates, sometimes called "democratic" coordinates, and are discussed in detail in Refs. [13–15]. The key to the adiabatic hyperspherical representation is that the dynamics of the three-body system, described by the hyperangles, is reduced to collective motion under the influence of one-dimensional effective potentials in R, which is governed by a system of ordinary differential equations similar to the usual radial Schrödinger equation for two-body systems.

The hyperspherical coordinates are introduced through the mass-scaled Jacobi coordinates $\vec{\rho}_1$ and $\vec{\rho}_2$ (see Fig. 1) defined as

$$\vec{\rho}_1 = (\vec{r}_2 - \vec{r}_1)/d,$$

$$\vec{\rho}_2 = d\left(\vec{r}_3 - \frac{m_1\vec{r}_1 + m_2\vec{r}_2}{m_1 + m_2}\right). \tag{1}$$

In the above equations $\vec{r}_i$ is the position of the particle i (of mass m_i) relative to a space-fixed frame. For three identical particles of mass m, we define a three-body reduced mass as $\mu = m/\sqrt{3}$, which gives $d = 2^{1/2}/3^{1/4}$ [14,15]. It is important to note that the hyperradius,

$$R^2 = \rho_1^2 + \rho_2^2, \quad R \in [0, \infty), \tag{2}$$

is an invariant quantity, i.e., it does not depend on the particular choice of the hyperangles or permutations of the particles. In fact, it turns out that permutation symmetry affects only φ, which greatly simplifies symmetrizing the wave function. This angle, along with θ, describe the internal motion of the system at a fixed R. In particular, the geometry of the system enters through these two angles with θ largely responsible for the shape of the three-body triangle.

The Schrödinger equation can be more conveniently written in terms of the rescaled wave function $\psi = R^{5/2}\Psi$, as

$$\left[-\frac{\hbar^2}{2\mu}\frac{\partial^2}{\partial R^2} + H_{\rm ad}(R,\Omega)\right]\psi(R,\Omega) = E\psi(R,\Omega), \tag{3}$$

where E is the total energy and $H_{\rm ad}$ is the adiabatic Hamiltonian given by

$$H_{\rm ad}(R,\Omega) = \frac{\hbar^2}{2\mu R^2}\left[\Lambda^2(\Omega) + \frac{15}{4}\right] + V(R,\varphi,\theta). \tag{4}$$

The adiabatic Hamiltonian $H_{\rm ad}$ contains all hyperangular dependence, represented collectively by $\Omega \equiv \{\varphi, \theta, \alpha, \beta, \gamma\}$, and includes the hyperangular kinetic energy in the grand angular momentum operator Λ^2 as well as all interparticle interactions V. An explicit definition for $H_{\rm ad}$ in terms of the hyperangles φ, θ, α, β, and γ can be found in Refs. [14,15].

In the adiabatic hyperspherical representation, the total wave function is expanded in terms of the channel functions $\Phi_\nu(R;\Omega)$,

$$\psi_n(R,\Omega) = \sum_\nu F_{n\nu}(R)\Phi_\nu(R;\Omega), \tag{5}$$

where $F_{n\nu}(R)$ are the hyperradial wave functions, n labels the different energy eigenstates for a given ν, and ν represents all remaining quantum numbers necessary to specify each channel. The channel functions $\Phi_\nu(R;\Omega)$ form a complete set of orthonormal functions at each value of R and are eigenfunctions of the adiabatic Hamiltonian:

$$H_{\rm ad}(R,\Omega)\Phi_\nu(R;\Omega) = U_\nu(R)\Phi_\nu(R;\Omega). \tag{6}$$

The eigenvalues $U_\nu(R)$ help define effective three-body potentials for the hyperradial motion.

Substituting Eq. (5) into the Schrödinger equation (3) and projecting out $\Phi_{\nu'}$, we obtain the hyperradial Schrödinger equation

$$\left[-\frac{\hbar^2}{2\mu}\frac{d^2}{dR^2} + U_\nu(R)\right]F_\nu(R) - \frac{\hbar^2}{2\mu}\sum_{\nu'}\left[2P_{\nu\nu'}(R)\frac{d}{dR} + Q_{\nu\nu'}(R)\right]F_{\nu'}(R) = EF_\nu(R), \tag{7}$$

which describes the motion of the three-body system under the influence of the effective potentials $U_\nu(R) - Q_{\nu\nu}(R)/2\mu$. In Eq. (7), the nonadiabatic coupling terms $P_{\nu\nu'}(R)$ and $Q_{\nu\nu'}(R)$ drive inelastic processes and are defined as

$$P_{\nu\nu'}(R) = \left\langle\left\langle \Phi_\nu \left| \frac{d}{dR} \right| \Phi_{\nu'} \right\rangle\right\rangle \tag{8}$$

and

$$Q_{\nu\nu'}(R) = \left\langle\left\langle \Phi_\nu \left| \frac{d^2}{dR^2} \right| \Phi_{\nu'} \right\rangle\right\rangle, \tag{9}$$

where the double brackets denote integration over the angular coordinates Ω only. As it stands, Eq. (7) is exact. In practice, of course, the sum over channels must be truncated. In fact, the accuracy of the solutions can be monitored with successively larger truncations since the bound state energies obtained at each stage are an upper bound by the variational principle. Neglecting all off-diagonal coupling in Eq. (7) decouples the equations and is called the adiabatic hyperspherical approximation. Discrete states in the lowest resulting effective potential become bound states of the system. Any discrete states in higher potentials that lie above the asymptotic threshold of the lowest potential become resonances of the system upon inclusion of the nonadiabatic coupling. In the analog atomic system—the helium atom—these resonances are the doubly excited states.

In this paper, we explore the solutions of the system of differential equations (7) for three particles with attractive $1/r$ interactions. We determine the effective potentials and couplings by solving Eq. (6) for the $J^\pi = 0^+$ symmetry, where

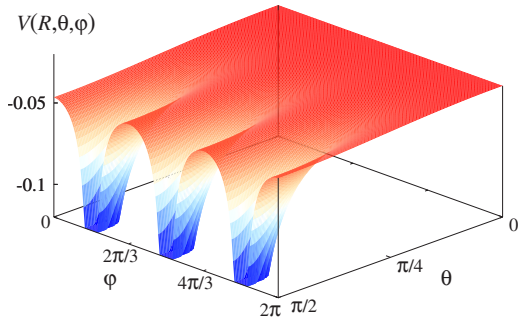

FIG. 2. (Color online) The potential $V(R,\theta,\varphi)$ at $R=100$. Due to the symmetry properties of the three identical particles, the adiabatic equation [Eq. (6)] is solved only for $\theta=0$ to $\pi/2$ and $\varphi=0$ to $2\pi/3$.

J is the total orbital angular momentum and π is the total parity. The bound state energies are then determined by solving Eq. (7). We characterize the resulting states from the asymptotic behavior $(R\to\infty)$ of the effective potentials $U_\nu(R)-Q_{\nu\nu}(R)/2\mu$ and from the channel functions $\Phi_\nu(R;\Omega)$, allowing us to determine, for instance, their geometry and vibrational motion.

In order to solve the adiabatic equation (6), we in general expand the channel functions $\Phi_\nu(R;\Omega)$ in terms of the Wigner D functions [14,16,17],

$$\Phi_\nu^{JM\pi}(R;\Omega)=\sum_K \phi_{K\nu}(R;\theta,\varphi)D^J_{KM}(\alpha,\beta,\gamma), \tag{10}$$

where K and M are the projection of $\vec{J}$ onto the body-fixed and space-fixed z axes, respectively. After projecting out the D functions, the resulting coupled system of partial differential equations for $\phi_{K\nu}(R;\theta,\varphi)$ is solved (for each value of R) by expanding $\phi_{K\nu}(R;\theta,\varphi)$ on a direct product of fifth-order basis splines [18] in the hyperangles θ and φ. For $J^\pi=0^+$, of course, the sum involves only one term, requiring the solution of a single two-dimensional partial differential equation.

The potential V in Eq. (4) is given by a pairwise sum of attractive $1/r$ potentials,

$$V(R,\theta,\varphi)=-\frac{u}{r_{12}}-\frac{u}{r_{23}}-\frac{u}{r_{31}}, \tag{11}$$

where u is the gravitationlike coupling. The interparticle distances r_{ij} are given in terms of the hyperspherical coordinates by

$$r_{12}=3^{-1/4}R[1+\sin\theta\sin(\varphi-\pi/6)]^{1/2},$$

$$r_{23}=3^{-1/4}R[1+\sin\theta\sin(\varphi-5\pi/6)]^{1/2},$$

$$r_{31}=3^{-1/4}R[1+\sin\theta\sin(\varphi+\pi/2)]^{1/2}. \tag{12}$$

For the present calculations, however, we base our units on u, thus producing a unitless equation. Our length units are $2\hbar^2/mu$, and our energy units are $mu^2/2\hbar^2$. These yield, in analogy to atomic units, a two-body energy spectrum $E_n=-1/2n^2$.

Figure 2 shows the potential $V(R,\theta,\varphi)$ as a function of θ and φ at $R=100$. The singular points at $\theta=\pi/2$ and $\varphi=\pi/3$, π and $5\pi/3$ are the points where $r_{23}=0$, $r_{31}=0$, and $r_{12}=0$, respectively. The figure clearly shows the primary reason for our using Smith-Whitten coordinates: the potential is periodic in φ for identical particles. As a consequence, symmetrizing the channel function $\phi(R;\theta,\varphi)$ for 0^+ can be accomplished with the boundary conditions in φ. (Recall that permutations affect only φ, so all permutational symmetry is in the channel function.) Therefore, for three identical bosons, the two-dimensional 0^+ equation [Eq. (6)] needs to be solved—ideally—only from $\varphi=0$ to $\pi/3$, with the requirement that the derivative of $\phi(R;\theta,\varphi)$ with respect to φ is zero at each boundary. For the present system, however, we have to allow for the cusp in the channel function due to the $1/r_{23}$ divergence as $r_{23}\to 0$, which does not allow us to impose the zero derivative condition at $\varphi=\pi/3$ where $r_{23}=0$. Instead, we solve Eq. (6) from $\varphi=0$ to $2\pi/3$ requiring the φ derivative to be zero at each boundary. A simple postsymmetrization procedure that extracts the functions that are even about $\varphi=\pi/3$ yields the completely symmetric solutions. Further, to accurately represent the cusp, we chose our spline functions such that they had a discontinuous first derivative in φ at $\varphi=\pi/3$ [18].

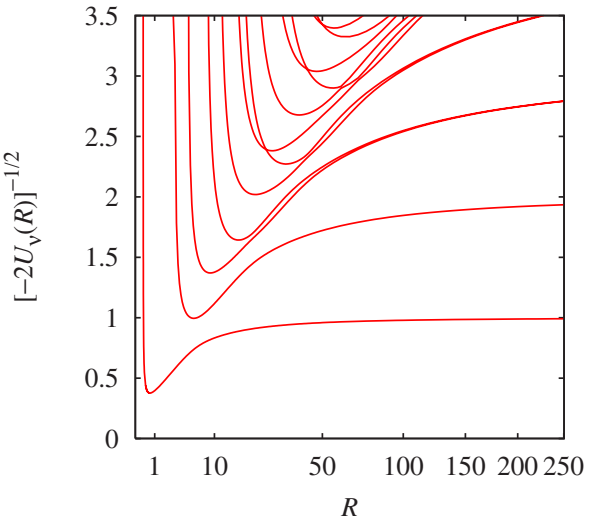

FIG. 3. (Color online) The hyperspherical potentials for three identical bosons with attractive $1/r$ interactions. For large values of R, $[-2U_\nu(R)]^{-1/2}$ converges to the principal quantum number n_{2b} for the hydrogenlike subsystems.

For the system suggested in Ref. [1], the coupling u [Eq. (11)] is given by [in Système International (SI) units]

$$u=\frac{11}{4\pi}\frac{Iq^2\alpha_p^2}{c\varepsilon_0^2},$$

where I is the laser intensity, q the photon wave number, and α_p the atomic dynamic polarizability. So, under the conditions discussed in Ref. [1], the strength of the interaction is controllable via the laser's parameters.

III. RESULTS AND DISCUSSION

Figure 3 shows the three-body potentials, calculated by solving Eq. (6), in the form $[-2U_\nu(R)]^{-1/2}$ such that for large

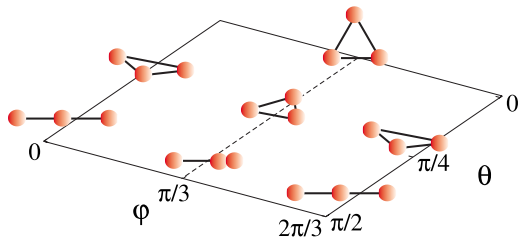

FIG. 4. (Color online) Three-body geometries as a function of the hyperangles θ and φ. $\theta=0$ corresponds to equilateral triangle configurations (irrespective to φ), while $\theta=\pi/2$ corresponds to collinear configurations.

values of R they converge to the principal quantum number n_{2b} associated with the two-body hydrogenlike subsystems (for $R\to\infty$ one particle is far from the others). The lowest potential in Fig. 3, converging to $n_{2b}=1$, supports the 0^+ bound states (or S^e, in analogy with atomic spectroscopic notation). In particular, it contains both the ground state and the S^e series of singly excited states, using the language of atomic structure. The higher potentials (converging to $n_{2b}>1$) support series of doubly excited states that are coupled to and can decay to the continuum of the lowest potential and are thus metastable. These comments draw on the similarity of these potentials to those for three-body systems like He and H^- [19]. There are minor differences, of course, due to the different permutational symmetries of the two systems and to the absence of the Coulomb repulsion for the present case.

As mentioned above, analysis of the asymptotic behavior of the effective potentials $U_\nu(R)-Q_{\nu\nu}(R)/2\mu$, calculated from the potentials shown in Fig. 3, makes it possible to determine the properties of the energy eigenstates of the system. In the present case, the effective potentials are asymptotically ($R\to\infty$) proportional to $1/R$. As a consequence, the main characteristics of the series of 0^+ bound states follow directly by identifying such states as Rydberg states. They are thus infinite in number, have binding energies that scale as $1/n^2$, and have sizes proportional to n^2. In this section, we will explicitly demonstrate the $1/n^2$ scaling for the binding energies. The presence of a Rydberg series in this system of neutral particles underscores its peculiar nature.

Since the $J^\pi=0^+$ channel functions (10) depend only on the hyperangles θ and φ they can be plotted in their entirety for each value of R. Figures 5 and 6 show the channel functions for the two lowest channels at $R=0.69$ and 100 for $\nu=1$, and $R=5.75$ and 100 for $\nu=2$. The first R value lies near the respective potential minima; and the second, in the asymptotic region. For small R, we plot Φ_ν in the range $0\le\varphi\le 2\pi/3$ from which the function in the whole range $0\le\varphi\le 2\pi$ can be obtained by symmetry (translation of the plotted portion by $2\pi/3$ and $4\pi/3$). For large R, however, we plot the solution only in the range $\pi/6\le\varphi\le\pi/2$ to show sufficient detail to see the two-body character of the solution.

The hyperangular distributions reveal both the geometry and vibrational motion of the system. For instance, the probable geometrical configuration for a channel function that displays a large probability in the θ-φ plane near $\theta=0$ is an

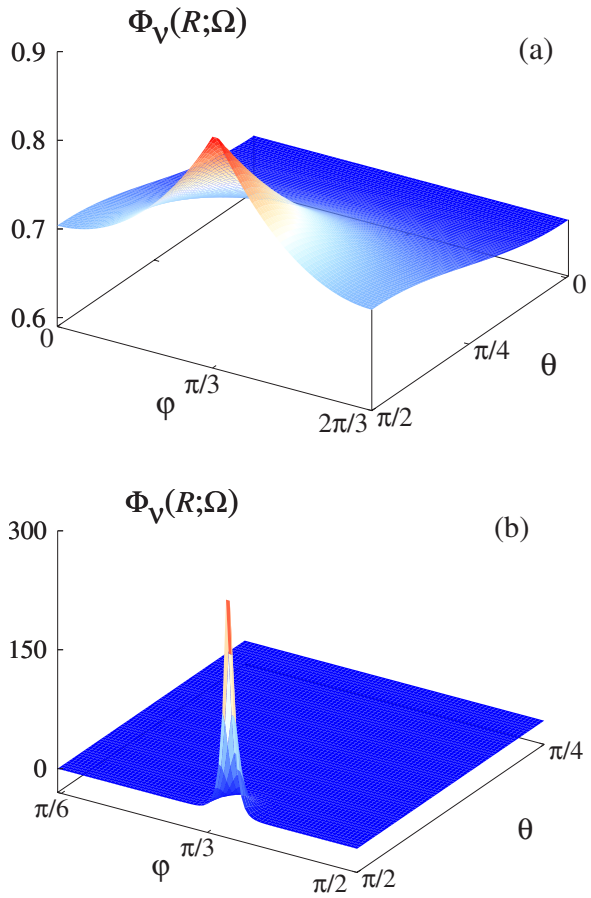

FIG. 5. (Color online) The lowest $J^\pi=0^+$ channel function ($\nu=1$) as a function of θ and φ at (a) $R=0.69$ and (b) $R=100$.

equilateral triangle. This can be easily seen from the definitions of the interatomic distances in Eq. (12), where for $\theta=0$ we have $r_{12}=r_{23}=r_{31}$. On the other hand, if the channel function peaks at $\theta=\pi/2$, the collinear configuration is most probable. In fact, from Eq. (12), for $\theta=\pi/2$ and $\varphi=\pi/3$, π and $5\pi/3$, corresponding to the two-body coalescence points $r_{23}=0$, $r_{31}=0$, and $r_{12}=0$, the geometry corresponds to a linear configuration with two of the particles closer to each other than to the third particle, representing strong two-body correlations. For $\varphi=0$, $2\pi/3$,$4\pi/3$, and 2π, though, the linear configuration has one of the atoms at the center of mass of the other two [see Eq. (12)].

The possible geometries as a function of θ and φ are summarized in Fig. 4. The equilateral configurations along $\theta=0$ in Fig. 4 are breathing modes whose size is determined by R. Motion along φ at $\theta=\pi/2$ takes the system through two possible collinear geometries representing antisymmetric vibration. As above, R scales every geometry, so symmetric vibration takes place in the R direction at fixed θ and φ. Motion in the θ direction at fixed φ [see Fig. 4] represents bending modes. Actual motion in any of these modes requires, of course, excitation. Otherwise, the state's behavior is governed by the hyperradial breathing motion.

In practice, of course, the channel functions are distributed over the whole θ-φ plane with some probability for each geometry. We can thus discuss only the most probable geometry (taking into account the $\sin 2\theta$ volume element). In Fig.

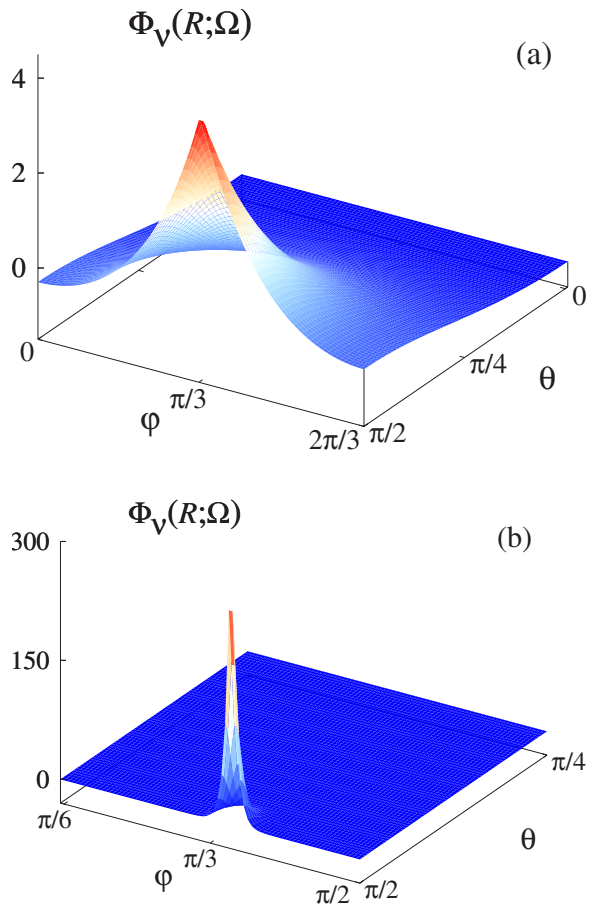

FIG. 6. (Color online) The first excited $J^\pi=0^+$ channel function ($\nu=2$) as a function of θ and φ at (a) $R=5.75$ and (b) $R=100$.

5(a) we show the channel function associated with the lowest potential ($\nu=1$) near its minimum (see Fig. 3). The channel function spreads out over the entire hyperangular plane with an increased amplitude near the two-body coalescence point ($r_{31}=0$ in the figure, and the others by symmetry) at $\theta=\pi/2$ and $\varphi=\pi/3$, corresponding to a linear configuration with two of the particles closer to each other than to the third particle (Fig. 4). Since this solution is nodeless, this state has primarily breathing-mode character in the radial direction. Therefore, all energy eigenstates associated with this channel should be breathing modes. As R increases [Fig. 5(b)], the channel function "collapses" to the region around the coalescence points, displaying the two-body character it must have for $R\to\infty$—in this case the $1s$ state.

Figures 6(a) and 6(b) show the $\nu=2$ channel function, which have much the same behavior as $\nu=1$ except for the necessary addition of a node. This node introduces motion in the hyperangles that is a combination of asymmetric vibration along $\theta=\pi/2$ and bending in the θ direction. There is a strong preference for equilateral triangles (due to the finite probability near $\theta=0$). Therefore, this channel—whose energy eigenstates are resonances in the continuum of the $\nu=1$ channel—describes rather complicated motion at smaller R, with the hyperradial motion contributing breathing (or symmetric stretching) in addition. As R increases, Fig. 6(b) shows that $\nu=2$ converges to the $2s$ state of the

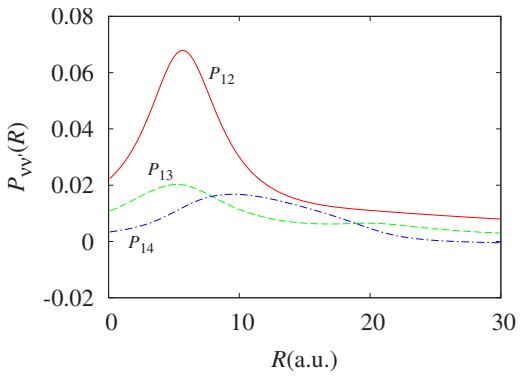

FIG. 7. (Color online) Nonadiabatic coupling $P_{\nu\nu'}$ between the lowest channel and the next three channels.

two-body subsystem in the collinear geometry for $\theta=\pi/2$ and $\varphi=\pi/3$. The motion in this limit is that of two particles orbiting each other far from the third which must lie near the collinear geometry. Note that for identical, spinless (or spin-stretched) bosons, $2p$ two-body states are not allowed by symmetry, so there is only a single potential correlating to $n_{2b}=2$ as $R\to\infty$.

Based on these observations, we conclude that the 0^+ bound states are primarily breathing modes, while the $\nu=1$ resonant states have bending-, stretching-, and breathing-mode contributions. Thus, bending modes can only contribute to the bound states through the nonadiabatic coupling, Eqs. (8) and (9), with higher channels. In our case, though, the channels are well separated in energy (see Fig. 3), and the coupling between them is expected to be small. This expectation will be confirmed below by calculating the eigenenergies and demonstrating that the contributions from higher channels are substantially smaller than from the ground channel.

In Ref. [20], the possible geometries and vibrational modes for three identical bosons with a repulsive core in their interaction were analyzed in detail. A rich geometrical structure was found along with a number of different modes. Thinking about the hyperangular probability distribution, a repulsive core would push the amplitude of the channel func-

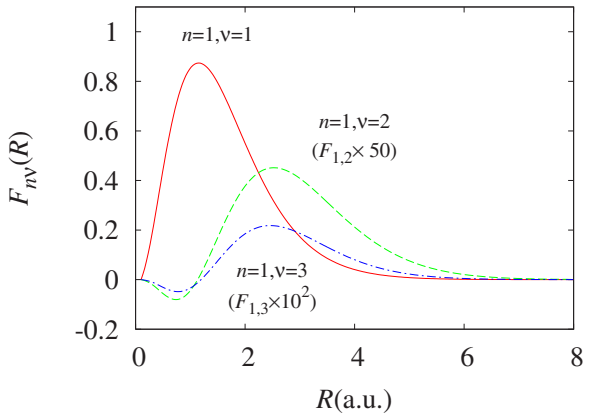

FIG. 8. (Color online) First three components of the ground-state hyperradial wave function $F_{n\nu}$ ($n=1$) associated with the first three channels $\nu=1$, 2, and 3.

TABLE I. The probability $\mathcal{P}_{n\nu}$ associated with the $\nu=1$ term of the expansion (5) for the ground state ($n=1$) and the next four excited states.

n	$\mathcal{P}_{n1}=\int_0^\infty \lvert F_{n1}\rvert^2 dR$
1	99.98%
2	99.80%
3	99.15%
4	98.90%
5	99.21%

tions in Figs. 5 and 6 away from the coalescence points, forcing the system to explore more of the shape space. A more complex geometrical and vibrational mode structure can thus be expected. In the same vein, the lack of a repulsive core in the present case likely leads to the simple geometry we have identified for all of the 0^+ bound states in the $\nu=1$ channel.

In Fig. 7 we show the nonadiabatic couplings $P_{\nu\nu'}(R)$ between the lowest channel and the next three channels ($P_{\nu\nu}=0$ and $P_{\nu\nu'}=-P_{\nu'\nu}$) calculated from Eq. (9). The fact that the coupling P_{12} in Fig. 7 is substantially larger than the couplings with higher channels implies rapid convergence for the bound-state energies as a function of the number of channels. Further, P_{12} peaks around $R=6$, which correlates roughly with the location of a weak avoided crossing between the corresponding potential curves as expected (see Fig. 3).

We have solved Eq. (7) and determined the bound-state energies and hyperradial wave functions $F_{n\nu}(R)$, including up to 15 channels. For example, Fig. 8 shows the ground-state wave function for a three channel calculation. The $\nu=1$ component is associated with the lowest adiabatic channel, while the $\nu=2$ and $\nu=3$ are related to the next two adiabatic channels and are present due to the coupling between the channels. Note that the probability given by $\mathcal{P}_{n\nu}=\int_0^\infty \lvert F_{n\nu}(R)\rvert^2 dR$ due to the first term dominates the other contributions. In Table I we show $\mathcal{P}_{n\nu=1}$ for the ground state ($n=1$) and the four lowest excited states for a 15 channel calculation. The $\nu=1$ adiabatic channel represents roughly 99% or more of the probability for each state, showing that the adiabatic expansion is, in fact, quite good.

In Table II we show the ground-state energy as a function

TABLE II. Convergence of the ground-state energy as a function of the number of channels included in Eq. (7).

Number of channels	Ground-state energy ($mu^2/\hbar^2$)
1	−2.136 033
2	−2.136 481
3	−2.136 523
4	−2.136 525
5	−2.136 526
6	−2.136 527
15	−2.136 527

TABLE III. Ground-state and excited-states energies $E_{n,\nu}$ ($\nu=1$) calculated using 15 coupled channels.

n	$E_{n,\nu}$ ($mu^2/\hbar^2$)
1	−2.136 527
2	−1.145 881
3	−0.786 454
4	−0.661 162
5	−0.603 740

of the number of channels, further demonstrating the expected rapid convergence of the adiabatic expansion. The ground-state energy for this system has been calculated before. In Ref. [12], for instance, a ground-state energy of $E_0\cong -1.067G^2m^5/\hbar^2=-2.134mu^2/\hbar^2$ (in our units) was obtained. Comparison with Table II shows that since both calculations are variational, our single channel calculation already gives a more precise result. We speculate that the large differences in the potential energies shown in Fig. 3 are the main reason that a single channel already gives such a good result. In fact, this channel separation is closely related to the small magnitude of the coupling terms shown in Fig. 7. Table II also shows that our six channel approximation for the ground state gives a result converged to seven digits.

Is well known [21] that the hyperspherical energy obtained disregarding all couplings and the energy obtained considering only the diagonal coupling in Eq. (7) are lower and upper bounds to the exact ground-state energy, respectively. In these approximations, we obtain a lower bound corresponding to $-2.138\,650\,mu^2/\hbar^2$ and an upper bound of $-2.136\,033mu^2/\hbar^2$. The difference between them is about 0.1%, while the bounds obtained in Ref. [12] give a difference of about 10%. By comparison, for a system such as the He atom [22], where the electronic repulsion plays an important role, the relative difference between the lower and upper bounds estimated from hyperspherical potential curves is about 1%.

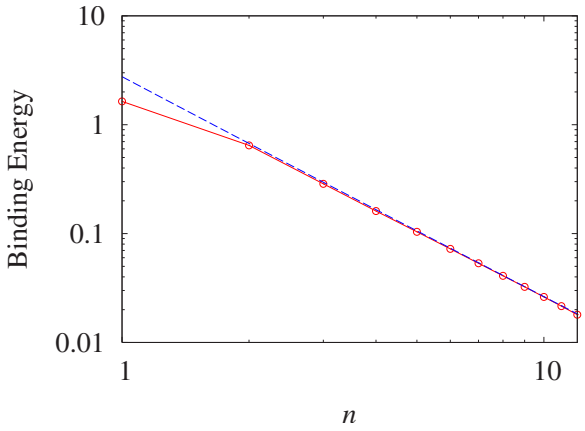

FIG. 9. (Color online) Binding energies for the ground state and the lowest 11 excited states of the 0^+ symmetry as a function of the principal quantum number n (dotted line). These results can be fit using the quantum defect formula $5.242\,94/[2(n-\delta)^2]$, with $\delta=0.026\,104\,9$ (dashed line).

In Table III we give our converged results for the ground and first four excited states (calculated with 15 channels), and in Fig. 9, we plot the binding energies for this series of states on a log-log scale, making evident the $1/n^2$ behavior typical of Rydberg states, as discussed above. The binding energies for $n>2$ can be fit using the quantum defect formula $5.242\,94/[2(n-\delta)^2]$, with $\delta=0.026\,104\,9$.

IV. SUMMARY

We have used the adiabatic hyperspherical representation to describe system of three identical bosons with attractive $1/r$ potentials. Such a system might eventually be created experimentally by irradiating ultracold atoms with intense, extremely off-resonant lasers. We calculated the ground-state and excited-state energies converged to seven digits which represents a substantial improvement over previous results. From our results for the effective potentials and binding energies, we have demonstrated that the bound states of the 0^+ symmetry form a Rydberg states and have given the corresponding quantum defect formula to calculate their energies. Our method is essentially exact, with the only approximation being the truncation of the number of channels used in the expansion of the total wave function. Although other methods—such as Hylleraas variational techniques—might provide *even* better bound states energies, as we have shown here the adiabatic hyperspherical representation naturally offers qualitative information along with quantitative results. For instance, we have used the adiabatic channel functions to determine the geometries of the 0^+ states. As a result, we have concluded that the 0^+ bound states are primarily breathing modes, while the lowest 0^+ resonant states have both bending and breathing mode contributions.

ACKNOWLEDGMENT

This work was supported by the National Science Foundation.

[1] D. O'Dell, S. Giovanazzi, G. Kurizki, and V. M. Akulin, Phys. Rev. Lett. **84**, 5687 (2000); see commentary by J. Anglin, Nature (London) **406**, 29 (2000).
[2] S. Giovanazzi, D. O'Dell, and G. Kurizki, Phys. Rev. A **63**, 031603(R) (2001).
[3] S. Giovanazzi, D. O'Dell, and G. Kurizki, Phys. Rev. Lett. **88**, 130402 (2002).
[4] D.-I. Choi, Phys. Rev. A **66**, 063609 (2002).
[5] V. S. Melezhik and C.-Y. Hu, Phys. Rev. Lett. **90**, 083202 (2003).
[6] S. Giovanazzi, G. Kurizki, I. E. Mazets, and S. Stringari, Europhys. Lett. **56**, 1 (2001).
[7] T. Thirunamachandran, Mol. Phys. **40**, 393 (1980); D. P. Craig and T. Thirunamachandran, *Molecular Quantum Electrodynamics* (Academic Press, London, 1984), Sec. 7.12.
[8] S. Inouye *et al.*, Nature (London) **392**, 151 (1998); J. Stenger, S. Inouye, M. R. Andrews, H. J. Miesner, D. M. Stamper-Kurn, and W. Ketterle, Phys. Rev. Lett. **82**, 2422 (1999).
[9] X. Z. Wang, Phys. Rev. D **64**, 124009 (2001).
[10] I. M. Moroz, R. Penrose, and P. Tod, Class. Quantum Grav. **15**, 2733 (1996).
[11] M. E. Fisher and D. Ruelle, J. Math. Phys. **7**, 260 (1966); F. J. Dyson and A. Lenard, *ibid.* **8**, 423 (1967).
[12] J. L. Basdevant, A. Martin, and J. M. Richard, Nucl. Phys. B **343**, 60 (1990).
[13] B. R. Johnson, J. Chem. Phys. **73**, 5051 (1980); **79**, 1906 (1983); **79**, 1916 (1980); R. C. Whitten and F. T. Smith, J. Math. Phys. **9**, 1103 (1968).
[14] H. Suno, B. D. Esry, C. H. Greene, and J. P. Burke, Jr., Phys. Rev. A **65**, 042725 (2002).
[15] H. Suno, B. D. Esry, and C. H. Greene, New J. Phys. **5**, 53 (2003).
[16] R. T Pack and G. A. Parker, J. Chem. Phys. **87**, 3888 (1987).
[17] M. E. Rose, *Elementary Theory of Angular Momentum* (Wiley, New York, 1957), pp. 52–54.
[18] C. de Boor, *A Practical Guide to Splines* (Springer, New York, 1978).
[19] C. D. Lin, Phys. Rep. **257**, 1 (1995).
[20] C. G. Bao *et al.*, Few-Body Syst. **2**, 81 (1987).
[21] A. F. Starace and G. L. Webster, Phys. Rev. A **19**, 1629 (1979); H. T. Coelho and J. E. Hornos, *ibid.* **43**, 6379 (1991).
[22] J. J. De Groote, M. Masili, and J. E. Hornos, J. Phys. B **31**, 4755 (1998).